Main Manuscript for

The androgen receptor in mesenchymal progenitors regulates skeletal muscle mass via *Igf1* expression in male mice.

Hiroshi Sakai[1,2,*], Hideaki Uno[2], Harumi Yamakawa[2], Kaori Tanaka[3], Aoi Ikedo[1], Akiyoshi Uezumi[4], Yasuyuki Ohkawa[3], Yuuki Imai[1,2,*]

[1]Division of Integrative Pathophysiology, Proteo-Science Center, Ehime University, Toon, Ehime 791-0295, Japan.

[2]Department of Pathophysiology, Ehime University Graduate School of Medicine, Toon, Ehime 791-0295, Japan.

[3]Division of Transcriptomics, Medical Institute of Bioregulation, Kyushu University, Higashi-ku, Fukuoka 812-0054, Japan.

[4]Divison of Cell Heterogeneity, Medical Institute of Bioregulation, Kyushu University, Higashi-ku, Fukuoka 812-0054, Japan.

[*]Hiroshi Sakai, Yuuki Imai

Hiroshi Sakai, DVM, PhD, and Yuuki Imai, MD, PhD, Proteo-Science Center, Graduate School of Medicine, Ehime University, Shitsukawa, Toon, Ehime, 791-0295, Japan.

+81-89-960-5925

Email: sakai.hiroshi.wh@ehime-u.ac.jp (H.S.), y-imai@m.ehime-u.ac.jp (Y.I.)

Author Contributions: Conceptualization, H.S. and Y.I.; Methodology, H.S., H.U., K.T., A.I., A.U., Y.O., and Y.I.; Software, H.S., H.U., and K.T.; Investigation, H.S., H.U., H.Y., K.T., and A.I.; Writing – Original Draft, H.S. and Y.I.; Writing – Review & Editing, H.S. and Y.I.; Funding Acquisition, H.S. and Y.I.; Resources, H.S., K.T., A.U., Y.O., and Y.I.; Supervision, H.S. and Y.I.

Competing Interest Statement: The authors declare no competing interests.

Keywords: androgen receptor, skeletal muscle, mesenchymal progenitors, Igf1

This PDF file includes:

Main Text

Figures 1 to 4

Abstract

Androgens exert their effects primarily by binding to the androgen receptor (AR), a ligand-dependent nuclear receptor. While androgens have anabolic effects on skeletal muscle, previous studies reported that AR functions in myofibers to regulate skeletal muscle quality, rather than skeletal muscle mass. Therefore, the anabolic effects of androgens are exerted via extra-myofiber cells or tissues. In this context, the cellular and molecular mechanisms of AR in mesenchymal progenitors, which play a crucial role in maintaining skeletal muscle homeostasis, remain largely unknown. In this study, we demonstrated expression of AR in mesenchymal progenitors and found that targeted AR ablation in mesenchymal progenitors reduced limb muscle mass in mature adult, but not young or aged, male mice, although fatty infiltration of muscle was not affected. The absence of AR in mesenchymal progenitors led to remarkable perineal muscle hypotrophy, regardless of age, due to abnormal regulation of transcripts associated with cell death and extracellular matrix organization. Additionally, we revealed that AR in mesenchymal progenitors regulates the expression of insulin-like growth factor 1 (Igf1), and that IGF1 administration prevents perineal muscles atrophy in a paracrine manner. These findings indicate that the anabolic effects of androgens regulate skeletal muscle mass via, at least in part, AR signaling in mesenchymal progenitors.

56 **Significance statement**

57 Androgens are essential not only for the development of male sexual characteristics but also for a
58 range of physiological functions, including the regulation of skeletal muscle growth and
59 function. Understanding the functionality of the androgen receptor (AR) is essential for
60 comprehending the mechanisms through which androgens exert their effects on skeletal muscles,
61 as these effects are mediated through AR binding. We demonstrate that AR is expressed in
62 mesenchymal progenitors, which play a vital role in muscle homeostasis, and regulates the
63 expression of insulin-like growth factor 1 (Igf1)—a key player in skeletal muscle growth—to
64 control muscle mass. Our study provides significant insights into potential therapeutic strategies
65 for addressing muscle atrophy conditions like sarcopenia.

Main Text

Introduction

Androgens are crucial regulators of various biological processes, including the development and maintenance of male characteristics. Notably, in a physiological context, the administration of androgens or androgen analogs has been shown to exert anabolic effects on muscles, resulting in increased muscle mass, strength, and body weight (1, 2). These physiological effects are mediated by activation of the androgen receptor (AR), a member of the nuclear receptor superfamily (3). However, despite that clinical administration of androgens in men can successfully increase skeletal muscle mass (4), the precise cellular and molecular mechanisms underlying the function of AR in muscle remain largely unexplored.

Skeletal muscle represents a complex tissue comprising multiple cell types, and the effects of androgens are likely mediated by various cell populations expressing AR within skeletal muscles. While male mice systemically lacking AR exhibit low skeletal muscle strength and mass, similar to female levels (5), we previously showed that muscle hypertrophy can be induced by androgen administration even in the absence of AR in myofibers, suggesting that non-myofiber AR contributes to the regulation of muscle mass (6). Furthermore, another of our studies demonstrated that deletion of AR in satellite cells, which are muscle stem cells responsible for muscle regeneration, had a limited effect on their proliferation and differentiation (7). Additionally, since limb muscle mass remains unaffected even in mice with AR ablation in both myofibers and muscle stem cells (8), other cells expressing AR within the muscles may play a role in regulating skeletal muscle mass.

Mesenchymal progenitors (9), also known as fibro/adipogenic progenitors (10), have been identified as a cell population distinct from myogenic cells characterized by the expression

89 of platelet-derived growth factor receptor alpha (PDGFRα). These cells are involved in the
90 maintenance and regeneration of skeletal muscle (11, 12). Conversely, mesenchymal progenitors
91 have been implicated in pathological fibrosis and fat accumulation in skeletal muscle (13). AR
92 expression has been reported in cells located in the interstitium or outside the basal lamina in
93 both mouse and human skeletal muscles (14, 15). Additionally, ablation of AR specifically in
94 embryonic cells of the mesenchyme led to impaired development of the perineal levator ani (LA)
95 and bulbocavernosus (BC) muscles (16), which are particularly responsive to androgen.
96 Furthermore, the reduced proliferation of undifferentiated myoblasts in these mutant mice
97 suggested a potential paracrine regulatory role of mesenchymal AR in controlling skeletal
98 muscles (16). Despite this knowledge, the specific role of AR in adult mesenchymal progenitors
99 in skeletal muscles remains unexplored.
100 Here we investigate the role of AR expressed in mesenchymal progenitors in muscle
101 maintenance using mice with mesenchymal progenitor-specific AR ablation. We show that AR
102 in mesenchymal progenitors plays a critical role in maintaining skeletal muscle mass via
103 regulation of insulin-like growth factor 1 (Igf1) expression in male mice.

Results

AR ablation in mesenchymal progenitors was validated in *PDGFRα-CreER;AR$^{L2/Y}$* mice

AR expression in fibroblasts of the perineal LA muscles and in mesenchymal cells of the fetal LA muscles has been reported (14, 16, 17); however, it is unknown whether mesenchymal progenitors in adult limb muscle express AR. To examine the expression pattern of AR in mesenchymal progenitors, immunofluorescence staining of PDGFRα, a marker of mesenchymal progenitors (9), and AR was performed in adult (12 weeks old) male mice. We found that AR was expressed in mesenchymal progenitors staining positive for PDGFRα (Fig. 1A), as well as in myofibers surrounded by laminin-expressing basal lamina, consistent with previous findings (17, 18).

To investigate the role of AR in mesenchymal progenitors, *PDGFRα-CreER* (19) and *AR$^{L2/Y}$* (20) mice were crossed to selectively delete the AR gene in mesenchymal progenitors expressing PDGFRα. Tamoxifen (TMX) was administered to Cre control male mice (*PDGFRα-CreER*) and mutant male mice (*PDGFRα-CreER;AR$^{L2/Y}$*) for 5 consecutive days to induce AR ablation (Fig. 1B). To assess the efficiency of AR ablation, immunofluorescence staining of PDGFRα and AR was performed in control and mutant mice. Quantification of PDGFRα and AR expression in forelimb biceps brachii (BB) and hindlimb tibialis anterior (TA) muscles demonstrated a significant decrease of 90% in AR protein in mutant mice compared with control mice, confirming successful ablation of AR expression in mesenchymal progenitors from *PDGFRα-CreER;AR$^{L2/Y}$* mice (Fig. 1C). In contrast, loss of AR in mesenchymal progenitors did not affect the number of PDGFRα+ cells (Fig. S1A). Taken together, these findings demonstrate successful and specific loss of AR expression in PDGFRα+ cells, rendering them an optimal model for investigating AR in mesenchymal progenitors in skeletal muscles.

127

128 **Lack of AR in mesenchymal progenitors had a limited effect on steady-state limb skeletal**
129 **muscles**

130 Because ablation of PDGFRα+ cells in intact muscles results in skeletal muscle atrophy (11, 12),
131 we first analyzed the muscles of control and mutant mice under steady-state conditions at a
132 young age (14 weeks old) (Fig. 1B). Body weight and limb skeletal muscle mass were not
133 affected in mutant compared with control mice at 2 weeks after TMX administration (Fig. S1B).
134 Moreover, the grip strength of mutant mice was comparable with that of control mice (Fig. S1C).
135 The minimum Ferret diameter, which is the robust parameter in order to measure myofiber size,
136 and number of myofibers in BB and TA muscles remained unchanged in mutant mice (Fig. S1D,
137 E). As relayed signaling between mesenchymal progenitors and muscle stem (satellite) cells is
138 critical for muscle hypertrophy (21), we also quantified the number of muscle stem cells.
139 Immunofluorescence staining of Pax7, a marker of muscle stem cells (22), revealed no difference
140 in the number of muscle stem cells between control and mutant BB and TA muscles (Fig. S1F).
141 We next investigated the fiber types of slow soleus muscles, which are affected by muscle fiber-
142 and muscle stem cell-specific AR ablation (8, 23). Analysis of soleus muscles fiber types by
143 immunofluorescence staining of type I (Myh7), type IIa (Myh2), and type IIx (without signals)
144 muscle fibers demonstrated no difference in the fiber-type parameters (minimum Ferret diameter
145 and frequency of each fiber-type) between control and mutant mice (Fig. S1G, H). Thus, AR
146 expression loss in mesenchymal progenitors has a limited effect on the steady-state limb muscles
147 of young mice.

148

149 **The impact of AR deficiency in mesenchymal progenitors on adipogenesis in muscles was**
150 **limited**

151 We also examined the adipogenesis of mesenchymal progenitors in mutant mice because
152 adipocytes originate from mesenchymal progenitors in skeletal muscles (9). To address this, both
153 the control and mutant mice were subjected to an 8-week regimen of high fat diet (HFD) feeding
154 (Fig. S2A). No significant differences were observed between the control mice and mutant mice
155 in terms of total body weight, hindlimb muscle weights, epididymal white adipose tissue
156 (eWAT) mass, and subcutaneous white adipose tissue (sWAT) mass (Fig. S2B), and grip
157 strength (Fig. S2C). Immunofluorescence staining of perilipin, a marker of adipocytes (24),
158 along with laminin, demonstrated no significant difference in the minimum Ferret diameter of
159 myofibers or the area occupied by adipocytes between the control and mutant TA muscles (Fig.
160 S2D, E).

161 To further investigate the impact of AR deficiency in muscle adipogenesis, we employed
162 a muscle injury model by administering glycerol injections into the TA muscle of both control
163 and mutant mice (Fig. S2F). No significant differences were observed between the control and
164 mutant mice in terms of the body and TA muscle weights at 2 weeks after injection (Fig. S2G).
165 Immunofluorescence staining of perilipin in conjunction with laminin (Fig. S2H) revealed no
166 significant difference in the minimum Ferret diameter of myofibers or the area occupied by
167 adipocytes between the control and mutant TA muscles (Fig. S2I). These findings suggest that
168 the absence of AR in mesenchymal progenitors does not significantly affect the adipogenic
169 properties of TA muscles.

170

171 **AR deficiency in mesenchymal progenitors affected limb skeletal muscles in mature adult**
172 **but not aged mice**
173 To investigate the effect of the duration of AR ablation on mesenchymal progenitors, we
174 analyzed mature adult (6 months old) mice and compared the Cre control group and mutant
175 group (Fig. 2A). In the mature adult mutant mice, we observed decreases in body weight, TA,
176 and gastrocnemius muscle weights (Fig. 2B), while there were no significant changes in the
177 weights of eWAT and sWAT (Fig. 2B), which are affected by systemic AR ablation (25).
178 However, grip strength (Fig. 2C) was comparable between the control and mutant mice.
179 Additionally, the weights of the entire body, hindlimb muscles, and white adipose tissues
180 were compared between aged (28 months old) control and mutant mice (Fig S2J). The aged
181 mutant mice did not exhibit any significant differences from the aged control mice (Fig. S2K and
182 S2L). Therefore, our findings demonstrate that AR deficiency in mesenchymal progenitors
183 affects skeletal muscle mass in mature adult mice only, not young or aged mice, primarily in the
184 limbs.
185
186 **Mesenchymal progenitor-specific AR ablation induced atrophy of LA/BC muscles**
187 The perineal LA/BC skeletal muscle complex exhibits increased responsiveness to androgens
188 compared with other striated muscles (26). Because this perineal muscle complex also has higher
189 AR expression (14), we examined the impact of AR ablation on mesenchymal progenitors of
190 LA/BC skeletal muscles. We confirmed efficient ablation of AR in PDGFRα+ cells in LA
191 muscles as well as limb muscles (Fig. 2D, E). We also found that AR depletion in mesenchymal
192 progenitors in LA muscles led to a decrease in the number of PDGFRα+ cells (Fig. 2F). At 14
193 weeks, 6 months, and 28 months of age, the LA/BC mass was consistently lower in the mutant

194 mice than control mice (Fig. 2G). Because AR ablation in myofibers using a promoter region
195 derived from the human α-skeletal actin (HSA) gene (*HSA-Cre;AR*$^{L2/Y}$ mice) also leads to
196 reduced LA/BC mass (27), we generated *HSA-Cre;PDGFRα-CreER;AR*$^{L2/Y}$ mice to examine
197 whether the weight reduction depended on AR in myofibers. Interestingly, the LA/BC weight
198 was lower in *HSA-Cre;AR*$^{L2/Y}$ mice than in *PDGFRα-CreER;AR*$^{L2/Y}$ mice (Fig. 2H). Moreover,
199 *HSA-Cre;PDGFRα-CreER;AR*$^{L2/Y}$ mice had the lowest LA/BC mass compared with *HSA-*
200 *Cre;AR*$^{L2/Y}$ and *PDGFRα-CreER;AR*$^{L2/Y}$ mice (Fig. 2G). These findings suggest that AR
201 expression in both myofibers and mesenchymal progenitors independently regulates the mass of
202 perineal muscles. Examination of the cross-sectional area (CSA) of LA muscles by laminin
203 staining (Fig. 2I) revealed a lower myofiber size and fewer myofibers in the mutant mice than
204 control mice (Fig. 2J). In summary, AR expression in mesenchymal progenitors independently
205 regulates the mass of perineal muscles, separate from its influence on myofibers.
206
207 **AR regulated genes related to extracellular matrix organization in mesenchymal**
208 **progenitors**
209 To determine the effects of AR on gene expression, we performed RNA-seq in PDGFRα+ cells
210 from the LA/BC muscles of both control and mutant mice (Fig. 3A). Using a previously
211 established gating strategy for isolating mesenchymal progenitors (CD45− CD31− Vcam1−
212 PDGFRα+) (12) (Fig. S3A), we isolated 300 PDGFRα+ cells from LA/BC muscles for RNA-
213 seq. We detected more than 100,000 genes in these cells, indicating sufficient read depth for
214 further analysis (Fig. S3B). The principal component analysis (PCA) plot showed separation
215 between the control and mutant samples (Fig. S3C). We identified 80 upregulated and 76
216 downregulated genes, including AR, in PDGFRα+ cells from the mutant mice (Fig. S3D). The

217 upregulated genes were enriched in the Gene Ontology (GO) terms including regulation of cell
218 death and cell motility (Fig. 3B). On the other hand, the downregulated genes were enriched in
219 the GO terms related to extracellular matrix (ECM) organization and regulation of proteolysis
220 (Fig. 3C).

221 To determine the AR target genes, we used CUT&RUN method for AR and trimethylated
222 lysine 4 from histone H3 (H3K4me3), which is enrich in active promoters, in mesenchymal
223 progenitors isolated from C57BL/6J male mice (Fig 3D), at 2 hours after treatment with
224 dihydrotestosterone (DHT), which was confirmed to induce AR expression in skeletal muscles
225 (Fig. S3E, S3F). We detected total 6542 peaks of AR in mesenchymal progenitors in skeletal
226 muscles. The AR peaks were primarily distributed in intron or intergenic regions (Fig. S3G),
227 similar to previous reports with AR ChIP-seq in muscle and non-muscle tissues (28, 29). We also
228 found the androgen response elements (ARE) in these peaks as the most enriched motif as well
229 as AR half-site (Fig. 3E, S3H). Moreover, AR CUT&RUN was validated by peaks found in the
230 *Fkbp5* locus (Fig. S3I), where canonical AR binding sites are located for several tissues (28). By
231 profiling AR peaks with AR and H3K4me3 reads, we found that AR binding sites were present
232 mainly not in promoter region (Fig. 3F). Furthermore, AR binding events were enriched for
233 regulation of locomotion and ECM organization GO terms (Fig. 3G). These results indicate that
234 AR in mesenchymal progenitors directly regulate the transcriptions including ECM organization
235 genes.

236

237 **AR in mesenchymal progenitors regulated *Igf1* expression**

238 To further investigate the gene regulation by AR in mesenchymal progenitors, we combined the
239 RNA-seq and CUT&RUN analysis. We found 39 genes which were downregulated in AR-

240 deficient mesenchymal progenitors and have AR peaks annotated by a nearest transcription start
241 sites (TSS) analysis (Fig. 4A). Top enriched GO term of these genes was ECM organization (Fig.
242 4B), including Collagen family (*Col1a1*, *Col3a1*, *Col4a1*, *Col4a2*, *Col5a1*, *Col5a2*, and *Col6a2*,
243 Fig. S4A and S4B), and *Igf1* (Fig. 4C), which is critical for maintaining muscle mass (30). We
244 also found the bindings of AR with ARE and peaks of H3K4me3 in upstream of *Igf1* TSS (Fig.
245 4D). Moreover, AR peaks were found with ARE in *Ar* gene locus (Fig. S4C), indicating the
246 regulation of *Ar* by AR in mesenchymal progenitors as other cells (31). To further investigate the
247 effects of androgen and AR on *Igf1* expression, we isolated PDGFRα+ cells from C57BL/6J
248 male mice treated with DHT (Fig. 4E). *Igf1* expression was upregulated in PDGFRα+ cells after
249 DHT administration (Fig. 4F). We also found reduction of IGF1 protein in the mutant LA
250 muscles (Fig. 4G and 4H). Finally, to determine whether the reduction in muscle mass in the
251 mutant mice was due to decreased IGF1 protein, we injected recombinant IGF1 into the LA/BC
252 muscles of the mutant mice just before TMX administration (Fig. 4I). We found that the mass of
253 the LA/BC muscles in IGF1-treated mutant mice increased compared to saline-injected mutant
254 mice, reaching levels comparable to those of saline-injected control mice (Fig. 4J).
255 Immunohistochemical staining of laminin in LA muscles (Fig. 4K) revealed a significant
256 reduction in muscle CSA of saline-injected mutant mice, which was prevented by IGF1 injection
257 (Fig. 4L). Additionally, the number of myofibers tended to decline following TMX
258 administration, and this trend was also mitigated by IGF1 injection (Fig. 4L). We also confirmed
259 that AR was efficiently ablated as early as 4 days after TMX treatment, and that IGF1 injection
260 did not impact the ablation efficiency (Fig. 4M). These findings indicate that IGF1 injection
261 effectively prevents the atrophy of LA/BC muscles in mutant mice. Taken together, AR in
262 mesenchymal progenitors regulates *Igf1* expression controlling skeletal muscle mass.

263 **Discussion**

264 In the present study, we demonstrated that male mice with specific AR ablation in mesenchymal
265 progenitors showed lower skeletal muscle mass in the limbs only at the mature adult stage, but
266 not at a younger stage (14 weeks old). Taken together with previous report demonstrating that
267 mice with AR ablation specifically in fast-twitch fibers lack muscle mass reduction at 13 weeks
268 old but exhibit this reduction at 12–13 months old (23), there may be an effect that requires time
269 to develop. Additionally, we demonstrated that the number of Pax7+ muscle stem cells was
270 similar between adult control and mutant mice. This is in contrast to the observed reduction in
271 myoblast proliferation following deletion of AR in the mesenchyme of BC muscles during
272 development (16), providing evidence that AR in mesenchymal progenitors plays distinct roles
273 during development, adulthood, and aging in mice. We also showed that specific ablation of AR
274 in mesenchymal progenitors does not affect the fiber types of slow-twitch muscles. Depletion of
275 mesenchymal progenitors results in a slight increase in the proportion of slow fibers (type I)
276 predominantly in fast-twitch TA muscles (12), suggesting that factors other than AR in
277 mesenchymal progenitors influence muscle fiber types. Muscle strength was either unaffected or
278 only slightly affected in myofiber-specific AR ablation mice (32), suggesting that non-myogenic
279 cells expressing AR may play a role in mediating muscle strength. However, grip strengths for
280 forelimbs were not affected in the mutant mice in all experimental groups conducted in present
281 study. Because the conventional grip strength test is influenced by various factors, including
282 inconsistent procedures and the motivation of the mice (33), more sensitive methods for
283 assessing muscle function, such as measuring in situ maximum isometric torque, and active and
284 passive force in skinned fibers (34), could detect subtle differences in muscle strength in the
285 mutant mice.

286 PDGFRα+ cells are the origin of ectopic adipocytes in skeletal muscles (9, 10). However,
287 the specific molecular mechanisms underlying fatty infiltration of muscles remain largely
288 unexplored (35). In general, androgen and AR signaling seem to have inhibitory effects on
289 adipogenesis (36). Serum androgens are linked to reduced levels of fatty infiltration of skeletal
290 muscles (37). In contrast, deprivation of androgens leads to an increase in fatty infiltration of
291 skeletal muscle in men (38). Moreover, transgenic mice expressing AR induced by collagen type
292 I alpha 1, which is also expressed in mesenchymal progenitors (39), have reduced body weight
293 and fat mass (40). Additionally, HFD-induced fat mass deposition in skeletal muscles was
294 increased by a low androgen level caused by orchidectomy (41). However, our results indicate
295 that AR deficiency in mesenchymal progenitors does not affect adipogenesis in skeletal muscle
296 even after HFD feeding or glycerol injection. An indirect androgen pathway may also regulate
297 adipogenesis of mesenchymal progenitors in skeletal muscles. Indeed, recent research indicates
298 that androgens can modulate macrophage polarization, subsequently affecting adipocyte
299 differentiation (42). Further studies are needed to gain a comprehensive understanding of the
300 mechanisms by which androgens and AR signaling influence fatty infiltration of muscle.
301 We observed a modest reduction in the muscle weight of the mutant mice at the mature
302 adult age (24 weeks old), but this effect was not observed in aged mice (28 months old). Because
303 selective ablation of AR in myofibers does not lead to reduced muscle mass even in 40-week-old
304 mice (27), the role of AR in mesenchymal progenitors is more important than its role in
305 myofibers in the context of muscle maintenance, at least at the mature adult age. The timing of
306 AR ablation could impact skeletal muscle mass, given the variation in initiation times for AR
307 ablation (tamoxifen treatment at 12 weeks old for analysis at 14 and 24 weeks, and at 8 weeks
308 old for analysis at 28 months). Experiments involving AR ablation at different ages, such as

309 TMX treatment at young (12 weeks old), mature adult (24 weeks old) and aged (24 months old)
310 mice, would help to clarify whether these results are influenced by age or the duration of AR
311 ablation. A decrease in testosterone concentration, even in 1-year-old mice compared with young
312 12-week-old mice (43), may contribute to muscle mass loss, potentially masking any subtle
313 differences between the aged control and mutant mice. Due to the reduction in muscle mass
314 observed in 2-year-old mice with AR depletion specifically in fast-twitch fibers (23), AR
315 expression in muscle fibers may play a crucial role in regulating muscle metabolism and quality,
316 which help maintain muscle mass in aged mice.

317 The perineal skeletal muscles LA and BC are highly androgen sensitive. Muscle fiber-
318 specific AR knockout results in a more pronounced mass reduction in LA/BC muscles compared
319 with limb muscles (26, 27), which is consistent with our present study demonstrating a severe
320 reduction in LA/BC muscles in mice with AR ablation in mesenchymal progenitors. We also
321 observed that the decrease in LA/BC weight in mice with AR ablation in mesenchymal
322 progenitors was less pronounced than in those with AR ablation in myofibers. Furthermore, the
323 double Cre mice (*HSA-Cre;PDGFRα-CreER;AR*$^{L2/Y}$), with ablation of AR in both myofibers and
324 mesenchymal progenitors, exhibited a greater reduction in LA/BC mass compared with single
325 Cre mice (*HSA-Cre;AR*$^{L2/Y}$ or *PDGFRα-CreER;AR*$^{L2/Y}$). Overexpression of AR in skeletal muscle
326 fibers using HSA promoter (44, 45) does not rescue the atrophy of LA muscles of testicular
327 feminization mutation (*Ar*^{Tfm}) male rat (45), supporting a separate role of AR in mesenchymal
328 progenitors for maintaining perineal muscle mass. Taken together, AR expression in
329 mesenchymal progenitors independently regulates the mass of perineal muscles, separate from
330 the influence of AR in myofibers. The distinct reactions observed in perineal and limb muscles
331 could be attributed to a greater abundance of myonuclei expressing AR in perineal muscles

332 compared with limb muscles (14). Nevertheless, our findings revealed that the majority of
333 PDGFRα+ cells exhibited AR expression in both limb and perineal muscles, suggesting an
334 additional mechanism by which AR in mesenchymal progenitors regulates muscle mass and
335 other mesenchymal progenitor functions.

336 AR ablation in PDGFRα+ cells in adult mice led to a reduction in both muscle CSA and
337 the number of myofibers in LA muscles. Additionally, our findings demonstrated that IGF1
338 injection into LA muscles protected against these reductions. Since age-related muscle loss, or
339 sarcopenia, is primarily characterized by a decrease in both the number and area of myofibers
340 (46), it is possible that the age-related decline in androgen levels, which results in reduced AR
341 expression in mesenchymal progenitors, contributes to these changes. Supporting this idea,
342 muscle-specific IGF1 overexpression in aged mice preserves myofiber numbers (47), while IGF1
343 receptor knockout in myofibers leads to a reduction in myofiber count (48), suggesting a critical
344 role for the AR/IGF1 axis in mesenchymal progenitors for maintaining myofibers. The reduction
345 of myofibers during aging is driven by various mechanisms, including satellite cell depletion,
346 altered protein synthesis, and increased muscle protein degradation (49). It's important to note
347 that the sensitivity of perineal muscles to androgens differs from that of limb muscles, suggesting
348 that distinct AR-mediated mechanisms may be responsible for maintaining myofibers in these
349 different muscle groups. Although our study found that genes related to cell death, which can
350 lead to decreased protein synthesis, were upregulated in mesenchymal progenitors of the perineal
351 LA/BC muscles following AR ablation, additional research is needed to elucidate the molecular
352 mechanisms by which AR/IGF1 axis dysfunction in mesenchymal progenitors contributes to
353 myofiber loss.

354 We also found that several ECM genes, including members of the collagen family, were
355 downregulated in AR-deficient mesenchymal progenitors, with AR peaks identified by a nearest
356 TSS analysis. These ECM components are primarily produced by PDGFRα+ cells in both
357 healthy and fibrotic skeletal muscles (39). AR expression promotes fibrosis in the heart, kidney,
358 and ovary (50–52), indicating that androgen/AR signaling governs ECM remodeling. Moreover,
359 downregulation of AR in PDGFRα+ fibroblasts from squamous cell carcinomas induces the
360 activation of cancer-associated fibroblasts (CAF), which remodel the ECM within the tumor
361 microenvironment (53). This suggests a general role for AR in PDGFRα+ cells under both
362 physiological and pathological conditions. Given that muscle diseases involving ECM
363 remodeling, such as muscular dystrophy and sarcopenia, are often accompanied by muscle
364 atrophy (54), it is plausible that ECM reduction due to AR deficiency contributes to skeletal
365 muscle atrophy. Further studies are needed to elucidate the relationship between AR, ECM, and
366 skeletal muscle plasticity.
367 The signaling pathway involving IGF1 plays a crucial role in both the developmental
368 growth and steady-state maintenance of skeletal muscle mass (55, 56). IGF1 is produced
369 primarily in the liver (57) but local production, including in skeletal muscles, is induced by
370 androgen treatment. The administration of testosterone to older men led to an increase in IGF1
371 protein expression in the limb (vastus lateralis) muscles (58). *Igf1* expression is decreased in the
372 LA/BC muscles of mice with skeletal muscle-specific AR ablation (27). Dubois et al. has
373 reported indirect androgen regulation of IGF1 via non myocytic AR because Myod-Cre-driven
374 AR-deficient mice showed no reduction in the *Igf1* transcript level, and *Igf1* expression was
375 decreased after castration in skeletal muscles (17). We demonstrated that AR in mesenchymal
376 progenitors in skeletal muscles regulated *Igf1* expression, governing muscle mass. Moreover,

377 activation of Akt signaling via the expression of Bmp3b in mesenchymal progenitors (12)
378 suggests a connection with Igf1, highlighting the complex interplay of signaling pathways in the
379 maintenance of skeletal muscle mass.

380 A limitation of our study in that we focused on male mice for studying AR in
381 mesenchymal progenitors of skeletal muscles. Because serum levels of androgens, including
382 testosterone and DHT, are also measurable in female mice (43), androgen/AR signaling could
383 potentially affect female skeletal muscles as well. Furthermore, *AR* was not differentially
384 expressed between males and females of human skeletal muscles (59), indicating potential roles
385 of AR in female skeletal muscles. On the other hand, genomic AR knockout mice show impaired
386 skeletal muscle development and function in males, but not females (5). Although muscle fiber-
387 specific AR knockout in female mice limitedly impacted on the expression of transcripts (6) and
388 muscle mass (23), more comparative work between male and female mice will be necessary to
389 determine whether AR plays important roles in female mesenchymal progenitors, as the function
390 of AR in these cells may differ from its role in female skeletal muscle fibers.

391 In summary, our results show that AR in mesenchymal progenitors regulates skeletal
392 muscle mass via *Igf1* expression (Fig. 4N). Further investigations into the limb muscles of aged
393 mice and humans are required to confirm whether combined treatment with androgens and IGF1
394 could be effective in treating muscle atrophy conditions such as sarcopenia.

395 **Materials and Methods**

396 **Animals**

397 *PDGFRα-CreER* mice (19), *HSA-Cre* mice (60), and C57BL/6J male mice were purchased from
398 Jackson Laboratories (Strain #: 018280, 006149, and 000664, respectively). $AR^{L2/Y}$ mice have
399 been described (20). *PDGFRα-CreER* male mice were crossed with $AR^{L2/+}$ female mice to
400 generate *PDGFRα-CreER;*$AR^{L2/Y}$ male mutant mice. Male littermates with the *PDGFRα-*
401 *CreER;*$AR^{+/Y}$ genotype were used as control mice. To generate *HSA-Cre;PDGFRα-CreER;*$AR^{L2/Y}$
402 male mice, *HSA-Cre* male mice were crossed with *PDGFRα-CreER;*$AR^{L2/+}$ female mice. All
403 mice were housed in a specific pathogen-free facility under climate-controlled conditions and a
404 12-hour light/dark cycle and were provided water and a standard diet *ad libitum*. In both control
405 and mutant mice, 100 μL of 20 mg/mL tamoxifen (TMX, Sigma-Aldrich, Cat# T5648),
406 dissolved in corn oil (Sigma-Aldrich, Cat# C8267), was injected intraperitoneally for 5
407 consecutive days at 8 or 12 weeks of age. A high-fat diet (HFD, CLEA Japan, Cat# HFD32) was
408 given *ad libitum* for 8 weeks to induce obesity in mice. The diet was refreshed every 2 days. To
409 induce fatty infiltration of skeletal muscle, 100 μL of 50% v/v glycerol was injected into tibialis
410 anterior (TA) muscles under anesthesia using isoflurane (61). To induce AR signaling, vehicle
411 (Veh) or dihydrotestosterone (DHT or stanolone, 2.5 mg/mouse; Tokyo Chemical Industry, Cat#
412 A0462), dissolved in absolute ethanol and diluted in 0.3% w/v hydroxypropyl cellulose (Wako,
413 Cat# 085-07932) in PBS, was injected subcutaneously into C57BL/6J male mice at 2 hours
414 before sampling. In *PDGFRα-CreER;*$AR^{L2/Y}$ male mutant mice, 10 μg/50 μL of recombinant
415 IGF1 (PeproTech, Cat# AF-100-11) dissolved in saline (Otsuka, Cat# 3311401A2026) or 50 μL
416 of saline was injected directly into LA/BC muscles for 4 consecutive days to keep the
417 concentration of IGF1 in the muscles at 12 weeks of age (62). The same amount of saline was

418 injected into LA/BC muscles of male littermates with the *PDGFRα-CreER;AR*$^{+/Y}$ genotype for
419 the control. TMX (100 μL of 20 mg/mL) was injected intraperitoneally, just after injection of
420 IGF1 or saline, for 4 consecutive days. All animal experiments were approved by the Animal
421 Experiment Committee of Ehime University (Approval No. 37A1-1·16) and were conducted in
422 full compliance with the Guidelines for Animal Experiments at Ehime University.
423

424 **Grip strength**

425 The grip strength of the forelimb was measured using a strain gauge (Melquest, Cat# GPM-
426 100B). The maximal force was determined after 10 measurements. The mean value recorded by
427 two independent experimenters was reported as the grip strength of each mouse.
428

429 **Immunofluorescence staining and microscopy**

430 For immunofluorescence staining, muscles were snap frozen in liquid nitrogen-chilled
431 isopentane. Cryosections of 10 μm thickness were prepared for immunofluorescence staining.
432 Sections were fixed in 4% paraformaldehyde in PBS for 5 min, blocked in 5% goat serum
433 (Gibco, Cat# 16210-064) in PBS for 60 min, and incubated with primary antibodies overnight at
434 4°C. For staining of myosin heavy chain (Myh), sections were air-dried and blocked with
435 M.O.M. reagent (Vector Laboratories, Cat# MKB-2213-1) at room temperature for 60 min.
436 Primary antibodies for Myh diluted in 1% BSA/PBS were incubated at 37°C for 45 min. The
437 antibodies used for immunofluorescence staining were anti-AR (Abcam, Cat# ab108341,
438 RRID:AB_10865716; 1/100), anti-PDGFRA (R&D Systems, Cat# AF1062,
439 RRID:AB_2236897; 1/80), anti-Laminin α2 (Santa Cruz Biotechnology, Cat# sc-59854,
440 RRID:AB_784266; 1/400), anti-Pax7 (DSHB, Cat# PAX7, RRID:AB_528428; 1/5), anti-

441 Laminin (Sigma-Aldrich, Cat# L9393, RRID:AB_477163; 1/500), anti-Myh7 (DSHB, Cat# BA-
442 D5, RRID:AB_2235587, supernatant; 1/100), anti-Myh2 (DSHB, Cat# SC-71,
443 RRID:AB_2147165, supernatant; 1/100), anti-Perilipin (Sigma-Aldrich, Cat# P1873,
444 RRID:AB_532267; 1/250), Alexa fluor 488 goat anti-rabbit IgG (Thermo Fisher Scientific, Cat#
445 A-11008; RRID:AB_143165; 1/1000), Alexa fluor 555 donkey anti-goat IgG (Thermo Fisher
446 Scientific, Cat# A-21432, RRID:AB_2535853; 1/1000), Alexa fluor 647 goat anti-rat IgG
447 (Thermo Fisher Scientific, Cat# A-21247, RRID:AB_141778; 1/1000), Alexa fluor 568 goat
448 anti-mouse IgG1 (Thermo Fisher Scientific, Cat# A-21124, RRID: AB_2535766; 1/1000), Alexa
449 fluor 488 goat anti-mouse IgG2b (Thermo Fisher Scientific, Cat# A-21141, RRID:AB_2535778;
450 1/1000), Alexa fluor 568 goat anti-rabbit IgG (Thermo Fisher Scientific, Cat# A-11011,
451 RRID:AB_143157; 1/1000), and Alexa fluor 647 goat anti-rabbit IgG (Thermo Fisher Scientific,
452 Cat# A27040; RRID:AB_143165; 1/1000). Nuclei were counterstained with DAPI. Entire cross
453 sections of fluorescence images were photographed using BIOREVO (Keyence) or Axio
454 Observer7 (Zeiss).
455
456 **Quantification of muscle sections**
457 To quantify the number, cross-sectional area (CSA), and minimum Ferret diameter of the
458 myofibers, captured images of entire cross sections were analyzed using Fiji (v2.3.0)
459 (https://imagej.net/Fiji). The myofiber area was identified by the laminin+ signals. The region of
460 interest (ROI) was set within the laminin+ areas. The frequency of each muscle fiber type in the
461 ROI was recorded by Trainable Weka Segmentation in Fiji after manual training. Small (< 150
462 μm^2) or large (> 10,000 μm^2) fibers were excluded for analyzing. The number of AR+PDGFRα+

463 mesenchymal progenitors, Pax7+ satellite cells, and the perilipin+ area was manually counted or
464 measured using Fiji.
465
466 **Isolation of mesenchymal progenitors from skeletal muscle**
467 Isolation of mononuclear cells from muscle was performed as described previously (63) with
468 minor modifications. Briefly, muscles were chopped in PBS on ice and digested using 800 U/mL
469 collagenase type 2 (Worthington, Cat# LS004177) in F10 medium (Gibco, Cat# 11550-043)
470 supplemented with 10% horse serum (Gibco, Cat# 26050-088) and antibiotic–antimycotic
471 (Gibco, Cat# 15240-062) for 60 min. Another digestion was conducted using 1000 U/mL
472 collagenase type 2 and 11 U/mL dispase (Gibco, Cat# 17105-041) for 30 min. The supernatants
473 were transferred to a 40 μm cell strainer (Falcon, Cat# 352340) to filter the debris and then
474 centrifuged to yield a cell suspension. The following antibodies were used: FITC anti-CD31
475 (BioLegend, Cat# 102406; RRID:AB_312901; 1/100), FITC anti-CD45 (BioLegend, Cat#
476 103108, RRID:AB_312973; 1/100), PE anti-VCAM1 (Thermo Fisher Scientific, Cat# 12-1061-
477 82, RRID:AB_2572573; 1/100), and APC anti-PDGFRα (R&D Systems, Cat# FAB1062A,
478 RRID:AB_3073817; 1/30). The BD FACSAria II (RRID:SCR_018091) or BD FACSAria
479 Fusion (BD Biosciences) was used for fluorescence-activated cell sorting (FACS), and the plot
480 was analyzed by FlowJo v10.1r7 (BD Life Sciences, RRID:SCR_008520).
481
482 **RNA-seq and data analysis**
483 For isolation of RNA from mesenchymal progenitors in LA/BC muscles, 300 PDGFRα+ cells
484 were sorted into the wells of a 96-well plate containing 10 μL lysis buffer at 4°C. The lysis
485 buffer was prepared by mixing 1 μL RNase inhibitor (Takara, Cat# 2313A) and 19 μL 10X lysis

486 buffer (Takara, Cat# 635013) diluted to 1X with nuclease-free water. 3' UTR RNA-seq was
487 conducted using the CEL-Seq2 protocol (64), with the exception of employing the Second Strand
488 Synthesis Module (New England Biolabs, Cat# E6111L) for double-stranded cDNA synthesis.
489 The library was then amplified via 10 cycles of PCR without any sample pooling. Subsequently,
490 the library was sequenced on the Illumina NovaSeq 6000, and quantitative analysis was
491 performed using 81 bp of insert reads (Read2).
492 Cell barcode and UMI information from Read1 were extracted using UMI-tools (v1.1.2)
493 (65) with the following command: "umi_tools extract -I read1.fastq --read2-in=read2.fastq --bc-
494 pattern=NNNNNNNNNNCCCCCCCCC". Adaptor and low-quality sequences were removed,
495 and reads with a length less than 20 bp were discarded using TrimGalore (v0.6.7;
496 http://www.bioinformatics.babraham.ac.uk/projects/trim_galore/). The processed reads were then
497 mapped to the GRCm38 reference genome using HISAT2 (v2.2.1) (66). Read counts for each
498 gene were obtained using featureCounts (v2.0.1) (67), and UMI duplications were removed
499 using UMI-tools. Four cell barcodes, "ATGCAATGC," "GACACGACA," "CGATGCGAT,"
500 and "TCTGGTCTG," were assigned to each sample. Differentially expressed genes were
501 identified using DESeq2 (v1.36.0) (68) with thresholds of |log2FC| > 1 and padj < 0.1.
502 Metascape (69) was used for Gene Ontology (GO) enrichment analysis.
503
504 **CUT&RUN and data analysis**
505 C57BL/6J male mice (10-12 weeks old) were treated with DHT at 2 hours before sampling for
506 FACS. For isolation of chromatin from mesenchymal progenitors in hindlimbs muscles, 500,000
507 PDGFRα+ cells were sorted to 20%FBS, DMEM/F12 (Gibco, Cat# 10565-018), Ultroser G
508 (Pall, Cat# 15950-017) supplemented with DHT (100 nM) to activate AR signaling during

509 sorting. After sorting, the nuclei were prepared with ChIC/CUT&RUN Assay Kit (Active Motif,
510 Cat# 53180) following the manufacturer's protocol. For AR (n = 4), H3K4me3 (n = 2), and IgG
511 control (n = 2) CUT&RUN, the following antibodies (1 µg/reaction) were used: anti-AR
512 (Abcam, Cat# ab108341, RRID:AB_10865716), anti-H3K4me3 (Active Motif, Cat# 39916,
513 RRID:AB_2687512), and rabbit negative control IgG (Active Motif, part of Cat# 53180). To
514 obtain enriched DNA after the CUT&RUN reaction, 20 µL of DNA purification elution buffer
515 was used instead of 55. The library was prepared using NEBNext Ultra II for DNA Library
516 Preparation for Illumina (New England Biolabs, Cat# E7645L) with some modifications
517 according to the Active Motif's instruction. All reactions were performed by half volume.
518 Constructed libraries were analyzed by 2100 Bioanalyzer using High Sensitivity DNA kit
519 (Agilent Technologies, Cat# 5067-4626), and quantified by qPCR using KAPA Library
520 Quantification Kits (Kapa Biosystems, Cat# KK4824). The library was sequenced on the
521 Illumina NovaSeq 6000 for 51 cycles of paired-end sequencing.
522 Paired-end reads were trimmed with TrimGalore and mapped to mm10 using Bowtie2
523 (v2.4.5) (70) with the following options: --no-mixed --no-discordant. Multi or no mate reads
524 were removed with samtools (v1.10) (71) view (-q 4 -F 0x2). To identify AR peaks across
525 samples, BAM files were merged across biological replicates (n = 2) to call peaks with MACS2
526 (v2.2.7.1) (-q 0.05) (72). H3K4me3 peaks were called on individual BAM files using MACS2 (-
527 q 0.0001). Merged BAM files for AR and IgG were used for downstream analysis (2 merged
528 BAM files for AR and 1 merged BAM file for IgG). Motif enrichment analysis of AR peaks was
529 performed with HOMER (v4.11) (73) findMotifs with -size 200 -mask options and AR peaks
530 were annotated to mm10 genes using annotatePeaks (-size 200 -mask) from MACS2 summit
531 files. Peaks distribution was annotated on mm10 (TxDb.Mmusculus.UCSC.mm10.knownGene,

532 R package version 3.4.7.) using ChIPpeakAnno package (v3.30.1) (74, 75) with MACS2
533 narrowPeak files. Promoter region was defined as 2000 bp upstream to 500 bp downstream of
534 transcription start sites (TSS). Common AR peaks-associated genes between replicates were
535 identified with Venn diagrams tools (http://bioinformatics.psb.ugent.be/webtools/Venn/). GO
536 enrichment analysis of common AR peaks-associated genes for GO Biological Process was
537 performed with Metascape. To generate bigwig files, merged (AR or IgG) or individual
538 (H3K4me3) BAM files were converted to CPM-normalized bigwig files using deepTools
539 (v3.5.1) (76) bamCoverage (--binSize 100 --normalizeUsing CPM). Peaks were visualized using
540 Integrative Genomics Viewer (IGV, v2.12.3) (77) with bigwig files. A count matrix for
541 aggregation plot was generated by deepTools computeMatrix reference-point (--skipZeros) with
542 AR and H3K4me3 bigwig files. Heatmaps were generated with count matrix files using
543 deepTools plotHeatmap.
544
545 **RNA isolation and quantitative real-time PCR**
546 C57BL/6J male mice (12 weeks old) were treated with Veh or DHT at 2 hours before sampling
547 for FACS, as described above. Total RNA was extracted from freshly sorted 30,000 PDGFRα+
548 cells from LA/BC muscles using the RNeasy Plus Micro Kit (Qiagen, Cat# 74034) following the
549 manufacturer's protocol. Reverse transcription was performed using PrimeScript (Takara, Cat#
550 RR036A) to synthesize cDNA from total RNA. Quantitative PCR (qPCR) was conducted in
551 technical duplicate samples utilizing TB Green Premix Ex Taq II (Takara, Cat# RR820S) and the
552 Thermal Cycler Dice (Takara, Cat# TP850). The expression levels of the target genes were
553 normalized to that of *Rpl13a*. The primer sequences are listed in Table S1.
554

555 **Western blotting**

556 LA muscles were dissolved in RIPA buffer (Fujifilm, Cat# 182-02451) supplemented with
557 protease inhibitors (Nacalai Tesque, Cat# 25955-11). Tissue-extracts were separated by SDS-
558 PAGE and transferred to polyvinylidene fluoride membranes. The membranes were blocked with
559 5% skim milk in TBS with Tween-20 (PBST), followed by incubation with anti-IGF1 (R&D
560 Systems, Cat# AF791, RRID:AB_2248752; 1/2000) or anti-GAPDH antibodies (Cell Signaling
561 Technology, Cat# 5174, RRID: AB_10622025; 1/1000) overnight at 4°C. The membranes were
562 incubated with an anti-goat (Agilent, Cat# P0160, 1:5000) or anti-rabbit immunoglobulin/HRP
563 secondary antibody (Agilent, Cat# P0448, RRID: AB_2617138; 1:5000) for 60 min at room
564 temperature. Signals were detected using ECL Prime Western Blotting Detection Reagents
565 (Amersham, Cat# RPN2232) on the Image Quant LAS 4000 system (GE Healthcare). Band
566 images were quantified by Fiji.

567

568 **Statistical analysis**

569 Prism 9 (GraphPad Software) or R (v4.0.5) (https://www.r-project.org) was used for the
570 statistical analysis. Welch's t-test was used to compare two groups. The two- or three-sample test
571 for equality of proportions was performed using the test of equal or given proportions. To
572 compare variables among three or more groups, Brown-Forsythe and Welch's ANOVA test with
573 Dunnett's T3 multiple comparison test was used.

Acknowledgments and funding sources

We are grateful to A. Nishio and Y. Sato for their technical support. We thank Y. Tanaka for the flow cytometry support, N. Tokunaga for the library preparations, and other members of the Division of Medical Research Support, the Advanced Research Support Center, Ehime University. This study was partly performed in the Cooperative Research Project Program in the Medical Institute of Bioregulation (MIB), Kyushu University. We also thank the Medical Research Center for High Depth Omics, MIB, Kyushu University for the sequencing, and RIST at Kyushu University for the high-performance computing. This work was supported in part by MEXT/JSPS KAKENHI (JP21K17568 to H.S.; JP22H03203 to Y.I.) and the HIRAKU-Global Program, which is funded by MEXT's "Strategic Professional Development Program for Young Researchers" and Takeda Science Foundation (to H.S.).

585 **Data Availability**

586 RNA-seq and CUT&RUN data have been deposited and are publicly available in the Gene

587 Expression Omnibus as accession number GSE247378.

588 **References**

589

590 1. G. N. Papanicolaou, E. A. Falk, General Muscular Hypertrophy Induced by Androgenic
591 Hormone. *Science* **87**, 238–239 (1938).

592 2. S. Bhasin, *et al.*, The Effects of Supraphysiologic Doses of Testosterone on Muscle Size and
593 Strength in Normal Men. *N. Engl. J. Med.* **335**, 1–7 (1996).

594 3. D. B. Lubahn, *et al.*, Cloning of Human Androgen Receptor Complementary DNA and
595 Localization to the X Chromosome. *Science* **240**, 327–330 (1988).

596 4. A. M. Lincoff, *et al.*, Cardiovascular Safety of Testosterone-Replacement Therapy. *N. Engl. J.*
597 *Med.* **389**, 107–117 (2023).

598 5. H. E. MacLean, *et al.*, Impaired skeletal muscle development and function in male, but not
599 female, genomic androgen receptor knockout mice. *FASEB J.* **22**, 2676–2689 (2008).

600 6. I. Sakakibara, *et al.*, Myofiber androgen receptor increases muscle strength mediated by a
601 skeletal muscle splicing variant of Mylk4. *iScience* **24**, 102303 (2021).

602 7. H. Sakai, T. Sato, M. Kanagawa, S. Fukada, Y. Imai, Androgen receptor in satellite cells is not
603 essential for muscle regenerations. *Exp. Results* **1** (2020).

604 8. V. Dubois, *et al.*, A satellite cell-specific knockout of the androgen receptor reveals myostatin
605 as a direct androgen target in skeletal muscle. *FASEB J.* **28**, 2979–2994 (2014).

606 9. A. Uezumi, S. Fukada, N. Yamamoto, S. Takeda, K. Tsuchida, Mesenchymal progenitors
607 distinct from satellite cells contribute to ectopic fat cell formation in skeletal muscle. *Nat. Cell*
608 *Biol.* **12**, 143–152 (2010).

609 10. A. W. B. Joe, *et al.*, Muscle injury activates resident fibro/adipogenic progenitors that
610 facilitate myogenesis. *Nat. Cell Biol.* **12**, 153–163 (2010).

611 11. M. N. Wosczyna, *et al.*, Mesenchymal Stromal Cells Are Required for Regeneration and
612 Homeostatic Maintenance of Skeletal Muscle. *Cell Rep.* **27**, 2029-2035.e5 (2019).

613 12. A. Uezumi, *et al.*, Mesenchymal Bmp3b expression maintains skeletal muscle integrity and
614 decreases in age-related sarcopenia. *J. Clin. Investig.* **131** (2020).

615 13. A. Uezumi, *et al.*, Fibrosis and adipogenesis originate from a common mesenchymal
616 progenitor in skeletal muscle. *J. Cell Sci.* **124**, 3654–3664 (2011).

617 14. J. A. Johansen, S. M. Breedlove, C. L. Jordan, Androgen Receptor Expression in the Levator
618 Ani Muscle of Male Mice. *J. Neuroendocr.* **19**, 823–826 (2007).

619 15. I. Sinha-Hikim, W. E. Taylor, N. F. Gonzalez-Cadavid, W. Zheng, S. Bhasin, Androgen
620 Receptor in Human Skeletal Muscle and Cultured Muscle Satellite Cells: Up-Regulation by
621 Androgen Treatment. *J. Clin. Endocrinol. Metab.* **89**, 5245–5255 (2004).

622 16. L. A. Ipulan, *et al.*, Nonmyocytic Androgen Receptor Regulates the Sexually Dimorphic
623 Development of the Embryonic Bulbocavernosus Muscle. *Endocrinology* **155**, 2467–2479
624 (2014).

625 17. V. Dubois, *et al.*, Enobosarm (GTx-024) Modulates Adult Skeletal Muscle Mass
626 Independently of the Androgen Receptor in the Satellite Cell Lineage. *Endocrinology* **156**, 4522–
627 4533 (2015).

628 18. M. Kanou, *et al.*, Polyamine pathway is associated with muscle anabolic effects by androgen
629 receptor ligand. *JCSM Rapid Commun.* **4**, 57–74 (2021).

630 19. S. H. Kang, M. Fukaya, J. K. Yang, J. D. Rothstein, D. E. Bergles, NG2+ CNS Glial
631 Progenitors Remain Committed to the Oligodendrocyte Lineage in Postnatal Life and following
632 Neurodegeneration. *Neuron* **68**, 668–681 (2010).

633 20. T. Matsumoto, K. Takeyama, T. Sato, S. Kato, Androgen receptor functions from reverse
634 genetic models. *J. Steroid Biochem. Mol. Biol.* **85**, 95–99 (2003).

635 21. A. Kaneshige, *et al.*, Relayed signaling between mesenchymal progenitors and muscle stem
636 cells ensures adaptive stem cell response to increased mechanical load. *Cell Stem Cell* **29**, 265-
637 280.e6 (2022).

638 22. P. Seale, *et al.*, Pax7 Is Required for the Specification of Myogenic Satellite Cells. *Cell* **102**,
639 777–786 (2000).

640 23. T. Hosoi, *et al.*, Sarcopenia phenotype and impaired muscle function in male mice with fast-
641 twitch muscle-specific knockout of the androgen receptor. *Proc. Natl. Acad. Sci. U.S.A.* **120**,
642 e2218032120 (2023).

643 24. A. S. Greenberg, *et al.*, Perilipin, a major hormonally regulated adipocyte-specific
644 phosphoprotein associated with the periphery of lipid storage droplets. *J. Biol. Chem.* **266**,
645 11341–11346 (1991).

646 25. W. Fan, *et al.*, Androgen Receptor Null Male Mice Develop Late-Onset Obesity Caused by
647 Decreased Energy Expenditure and Lipolytic Activity but Show Normal Insulin Sensitivity With
648 High Adiponectin Secretion. *Diabetes* **54**, 1000–1008 (2005).

649 26. J. Ophoff, *et al.*, Androgen Signaling in Myocytes Contributes to the Maintenance of Muscle
650 Mass and Fiber Type Regulation But Not to Muscle Strength or Fatigue. *Endocrinology* **150**,
651 3558–3566 (2009).

652 27. C. Chambon, *et al.*, Myocytic androgen receptor controls the strength but not the mass of
653 limb muscles. *Proc. Natl. Acad. Sci. U.S.A.* **107**, 14327–14332 (2010).

654 28. P. Pihlajamaa, *et al.*, Tissue-specific pioneer factors associate with androgen receptor
655 cistromes and transcription programs. *EMBO J.* **33**, 312–326 (2014).

656 29. K. Ghaibour, *et al.*, Androgen receptor coordinates muscle metabolic and contractile
657 functions. *J. Cachexia, Sarcopenia Muscle* **14**, 1707–1720 (2023).

658 30. C. Rommel, *et al.*, Mediation of IGF-1-induced skeletal myotube hypertrophy by
659 PI(3)K/Akt/mTOR and PI(3)K/Akt/GSK3 pathways. *Nat. Cell Biol.* **3**, 1009–1013 (2001).

660 31. J. M. Grad, L. S. Lyons, D. M. Robins, K. L. Burnstein, The Androgen Receptor (AR)
661 Amino-Terminus Imposes Androgen-Specific Regulation of AR Gene Expression via an Exonic
662 Enhancer. *Endocrinology* **142**, 1107–1116 (2001).

663 32. F. Jardí, *et al.*, Androgen and estrogen actions on male physical activity: a story beyond
664 muscle. *J. Endocrinol.* **238**, R31–R52 (2018).

665 33. H. Takeshita, *et al.*, Modified forelimb grip strength test detects aging-associated
666 physiological decline in skeletal muscle function in male mice. *Sci. Rep.* **7**, 42323 (2017).

667 34. T. Yamada, Y. Ashida, D. Tatebayashi, K. Himori, Myofibrillar function differs markedly
668 between denervated and dexamethasone-treated rat skeletal muscles: Role of mechanical load.
669 *PLoS ONE* **14**, e0223551 (2019).

670 35. M. W. Hamrick, M. E. McGee-Lawrence, D. M. Frechette, Fatty Infiltration of Skeletal
671 Muscle: Mechanisms and Comparisons with Bone Marrow Adiposity. *Front. Endocrinol.* **7**, 69
672 (2016).

673 36. J. Rizk, R. Sahu, D. Duteil, An overview on androgen-mediated actions in skeletal muscle
674 and adipose tissue. *Steroids* **199**, 109306 (2023).

675 37. I. Miljkovic, *et al.*, Bioactive androgens and glucuronidated androgen metabolites are
676 associated with subcutaneous and ectopic skeletal muscle adiposity among older black men.
677 *Metabolism* **60**, 1178–1185 (2011).

678 38. D. Chang, *et al.*, Androgen deprivation muscle attenuation. *J. Méd. Imaging Radiat. Oncol.*
679 **58**, 223–228 (2014).

680 39. M. A. Chapman, K. Mukund, S. Subramaniam, D. Brenner, R. L. Lieber, Three distinct cell
681 populations express extracellular matrix proteins and increase in number during skeletal muscle
682 fibrosis. *Am. J. Physiol. Cell Physiol.* **312**, C131–C143 (2017).

683 40. A. A. Semirale, X. Zhang, K. M. Wiren, Body composition changes and inhibition of fat
684 development in vivo implicates androgen in regulation of stem cell lineage allocation. *J. Cell.*
685 *Biochem.* **112**, 1773–1786 (2011).

686 41. V. Dubois, *et al.*, Androgen Deficiency Exacerbates High-Fat Diet-Induced Metabolic
687 Alterations in Male Mice. *Endocrinology* **157**, 648–665 (2016).

688 42. X. Ren, *et al.*, Testosterone regulates 3T3-L1 pre-adipocyte differentiation and epididymal
689 fat accumulation in mice through modulating macrophage polarization. *Biochem. Pharmacol.*
690 **140**, 73–88 (2017).

691 43. M. E. Nilsson, *et al.*, Measurement of a Comprehensive Sex Steroid Profile in Rodent Serum
692 by High-Sensitive Gas Chromatography-Tandem Mass Spectrometry. *Endocrinology* **156**, 2492–
693 2502 (2015).

694 44. D. A. Monks, *et al.*, Overexpression of wild-type androgen receptor in muscle recapitulates
695 polyglutamine disease. *Proc. Natl. Acad. Sci. U.S.A.* **104**, 18259–18264 (2007).

696 45. L. Niel, *et al.*, Sexual Differentiation of the Spinal Nucleus of the Bulbocavernosus Is Not
697 Mediated Solely by Androgen Receptors in Muscle Fibers. *Endocrinology* **150**, 3207–3213
698 (2009).

699 46. J. Lexell, C. C. Taylor, M. Sjöström, What is the cause of the ageing atrophy? Total number,
700 size and proportion of different fiber types studied in whole vastus lateralis muscle from 15- to
701 83-year-old men. *J. Neurol. Sci.* **84**, 275–294 (1988).

702 47. F. Ascenzi, *et al.*, Effects of IGF-1 isoforms on muscle growth and sarcopenia. *Aging Cell*
703 **18**, e12954 (2019).

704 48. M. D. Mavalli, *et al.*, Distinct growth hormone receptor signaling modes regulate skeletal
705 muscle development and insulin sensitivity in mice. *J. Clin. Investig.* **120**, 4007–4020 (2010).

706 49. H. Nishikawa, *et al.*, Pathophysiology and mechanisms of primary sarcopenia (Review). *Int.*
707 *J. Mol. Med.* **48**, 156 (2021).

708 50. Y. Wang, *et al.*, Androgen receptor regulates cardiac fibrosis in mice with experimental
709 autoimmune myocarditis by increasing microRNA-125b expression. *Biochem. Biophys. Res.*
710 *Commun.* **506**, 130–136 (2018).

711 51. S. Allam, *et al.*, Androgen receptor blockade by flutamide down-regulates renal fibrosis,
712 inflammation, and apoptosis pathways in male rats. *Life Sci.* **323**, 121697 (2023).

713 52. D. Wang, *et al.*, Bromodomain-containing protein 4 activates androgen receptor transcription
714 and promotes ovarian fibrosis in PCOS. *Cell Rep.* **42**, 113090 (2023).

715 53. A. Clocchiatti, *et al.*, Androgen receptor functions as transcriptional repressor of cancer-
716 associated fibroblast activation. *J. Clin. Investig.* **128**, 5531–5548 (2018).

717 54. O. Contreras, F. M. V. Rossi, M. Theret, Origins, potency, and heterogeneity of skeletal
718 muscle fibro-adipogenic progenitors—time for new definitions. *Skelet. Muscle* **11**, 16 (2021).

719 55. B. T. O'Neill, *et al.*, Insulin and IGF-1 receptors regulate FoxO-mediated signaling in muscle
720 proteostasis. *J. Clin. Invest.* **126**, 3433–3446 (2016).

721 56. F. Ascenzi, *et al.*, Effects of IGF-1 isoforms on muscle growth and sarcopenia. *Aging Cell*
722 **18**, e12954 (2019).

723 57. R. D. Kineman, M. del Rio-Moreno, A. Sarmento-Cabral, 40 YEARS of IGF1:
724 Understanding the tissue-specific roles of IGF1/IGF1R in regulating metabolism using the
725 Cre/loxP system. *J. Mol. Endocrinol.* **61**, T187–T198 (2018).

726 58. A. A. Ferrando, *et al.*, Testosterone administration to older men improves muscle function:
727 molecular and physiological mechanisms. *Am. J. Physiol. Endocrinol. Metab.* **282**, E601–E607
728 (2002).

729 59. C. M. Lopes-Ramos, *et al.*, Sex Differences in Gene Expression and Regulatory Networks
730 across 29 Human Tissues. *Cell Rep.* **31**, 107795 (2020).

731 60. P. Miniou, *et al.*, Gene targeting restricted to mouse striated muscle lineage. *Nucleic Acids*
732 *Res.* **27**, e27–e30 (1999).

733 61. N. Arsic, *et al.*, Vascular endothelial growth factor stimulates skeletal muscle regeneration in
734 Vivo. *Mol. Ther.* **10**, 844–854 (2004).

735 62. K. J. B. Martins, *et al.*, Intramuscular administration of PEGylated IGF-I improves skeletal
736 muscle regeneration after myotoxic injury. *Growth Horm. IGF Res.* **23**, 128–133 (2013).

737 63. L. Liu, T. H. Cheung, G. W. Charville, T. A. Rando, Isolation of skeletal muscle stem cells
738 by fluorescence-activated cell sorting. *Nat. Protoc.* **10**, 1612–1624 (2015).

739 64. T. Hashimshony, *et al.*, CEL-Seq2: sensitive highly-multiplexed single-cell RNA-Seq.
740 *Genome Biol.* **17**, 77 (2016).

741 65. T. Smith, A. Heger, I. Sudbery, UMI-tools: modeling sequencing errors in Unique Molecular
742 Identifiers to improve quantification accuracy. *Genome Res.* **27**, 491–499 (2017).

743 66. D. Kim, J. M. Paggi, C. Park, C. Bennett, S. L. Salzberg, Graph-based genome alignment and
744 genotyping with HISAT2 and HISAT-genotype. *Nat. Biotechnol.* **37**, 907–915 (2019).

745 67. Y. Liao, G. K. Smyth, W. Shi, featureCounts: an efficient general purpose program for
746 assigning sequence reads to genomic features. *Bioinformatics* **30**, 923–930 (2014).

747 68. M. I. Love, W. Huber, S. Anders, Moderated estimation of fold change and dispersion for
748 RNA-seq data with DESeq2. *Genome Biol.* **15**, 550 (2014).

749 69. Y. Zhou, *et al.*, Metascape provides a biologist-oriented resource for the analysis of systems-
750 level datasets. *Nat. Commun.* **10**, 1523 (2019).

751 70. B. Langmead, S. L. Salzberg, Fast gapped-read alignment with Bowtie 2. *Nat. Methods* **9**,
752 357–359 (2012).

753 71. P. Danecek, *et al.*, Twelve years of SAMtools and BCFtools. *GigaScience* **10**, giab008
754 (2021).

755 72. Y. Zhang, *et al.*, Model-based analysis of ChIP-Seq (MACS). *Genome Biol.* **9**, R137 (2008).

756 73. S. Heinz, *et al.*, Simple Combinations of Lineage-Determining Transcription Factors Prime
757 cis-Regulatory Elements Required for Macrophage and B Cell Identities. *Mol. Cell* **38**, 576–589
758 (2010).

759 74. L. J. Zhu, *et al.*, ChIPpeakAnno: a Bioconductor package to annotate ChIP-seq and ChIP-
760 chip data. *BMC Bioinform.* **11**, 237 (2010).

761 75. L. J. Zhu, Tiling Arrays, Methods and Protocols. *Methods Mol. Biol.* **1067**, 105–124 (2013).

762 76. F. Ramírez, *et al.*, deepTools2: a next generation web server for deep-sequencing data
763 analysis. *Nucleic Acids Res.* **44**, W160–W165 (2016).

764 77. J. T. Robinson, *et al.*, Integrative genomics viewer. *Nat. Biotechnol.* **29**, 24–26 (2011).

765

766

767 **Figures**

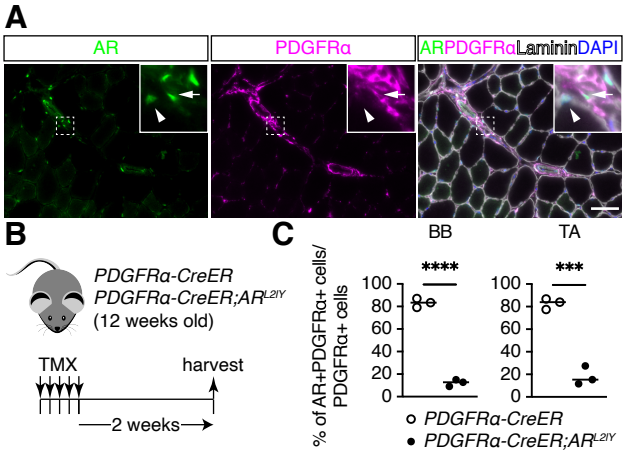

768

769 **Figure 1.** AR ablation in mesenchymal progenitors from *PDGFRα-CreER;AR$^{L2/Y}$* mice. (A)
770 Immunofluorescence staining of AR (left) and PDGFRα (middle) and of both together with
771 laminin and DAPI staining (right) in male TA muscles. Arrows: AR+ and PDGFRα+ cells;
772 arrowheads: AR+ nuclei surrounded by laminin. Scale bar, 50 µm. (B) Experimental design for
773 tamoxifen (TMX) treatment followed by sample harvest. (C) Quantification of AR+ cells among
774 PDGFRα+ cells in the biceps brachii (BB, left) and tibialis anterior (TA, right) muscles of
775 control and mutant mice (n = 3). The two-sample test for equality of proportions: ***$p < 0.001$,
776 ****$p < 0.0001$.

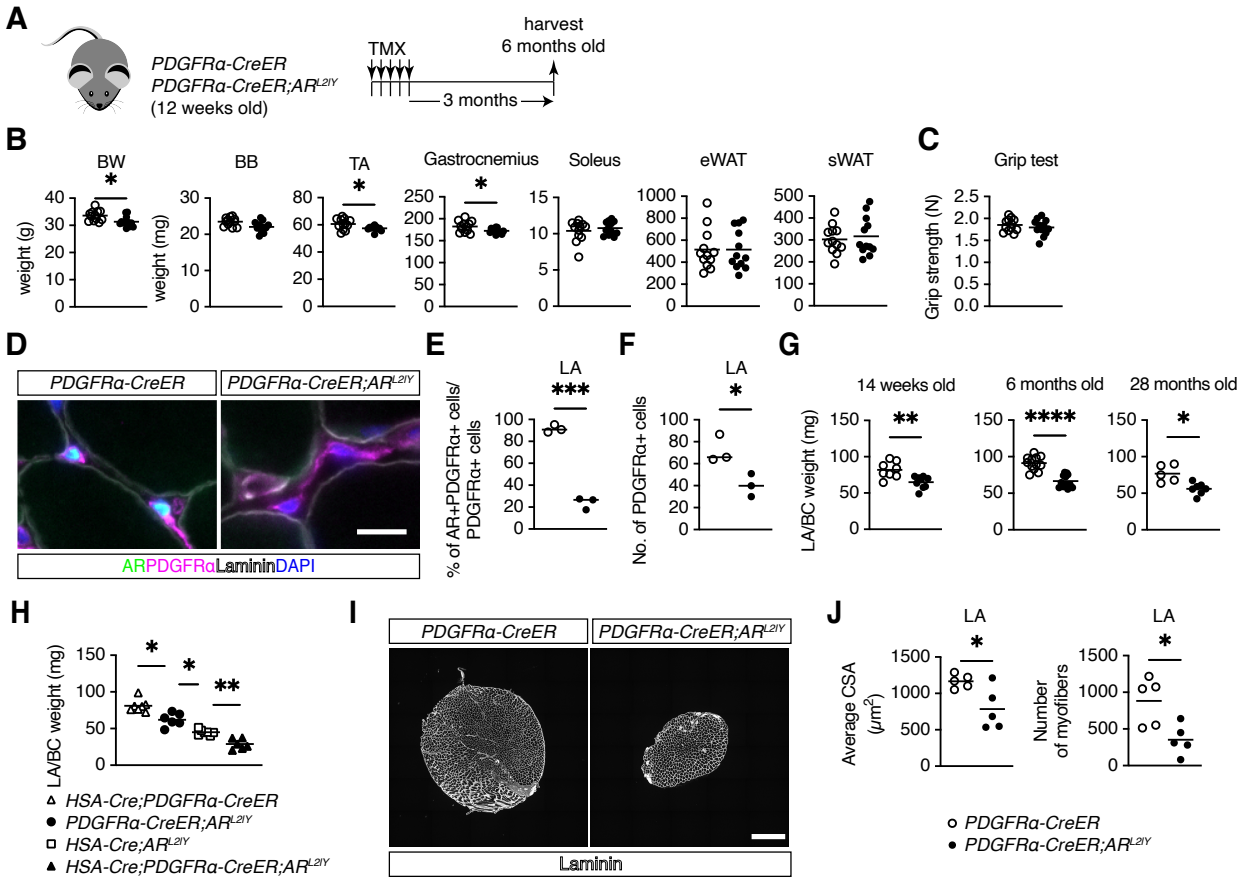

Figure 2. Atrophy of skeletal muscles in mesenchymal progenitor-specific AR-deficient mice. (A) Experimental design for tamoxifen (TMX) treatment followed by sample harvest in mature adult (6 months old) mice. (B and C) Quantification of body weight (BW), muscle mass, epididymal white adipose tissue (eWAT) mass, and subcutaneous WAT (sWAT) mass (B), and grip strength (C) in 6-month-old mice (n = 12). TA, tibialis anterior; BB, biceps brachii. Unpaired t-test with Welch's correction. (D) Immunofluorescence staining of AR, PDGFRα, and laminin with DAPI in levator ani (LA) muscles of control (left) and mutant (right) mice. Scale bar, 10 μm. (E) Quantification of AR+ cells among PDGFRα+ cells in LA muscles of control and mutant mice (n = 3). The two-sample test for equality of proportions. (F) Quantification of PDGFRα+ cells in LA muscles of control and mutant mice (n = 3). Unpaired t-test with Welch's correction. (G) Mass of LA and bulbocavernosus (BC) muscles in 14-week- (n = 8 control; n = 9

789 mutant mice), 6-month- (n = 12), and 28-month-old mice (n = 5 control; n = 7 mutant mice).
790 Unpaired t-test with Welch's correction. (H) Mass of LA/BC muscles in single (*HSA-Cre* or
791 *PDGFRα-CreER*) and double Cre mice (n = 7 *HSA-Cre;PDGFRα-CreER* and *HSA-Cre;AR*$^{L2/Y}$; n
792 = 6 mutant and *HSA-Cre;PDGFRα-CreER;AR*$^{L2/Y}$ mice). Brown-Forsythe and Welch's ANOVA
793 test with Dunnett's T3 multiple comparison test. (I) Immunofluorescence staining of laminin in
794 LA muscles of control (left) and mutant mice (right). Scale bar, 500 µm. (J) Average cross-
795 sectional area (CSA) (left) and the number of myofibers (right) in control and mutant mice (n =
796 5). Unpaired t-test with Welch's correction: *$p < 0.05$, **$p < 0.01$, ***$p < 0.001$, ****$p <$
797 0.0001.

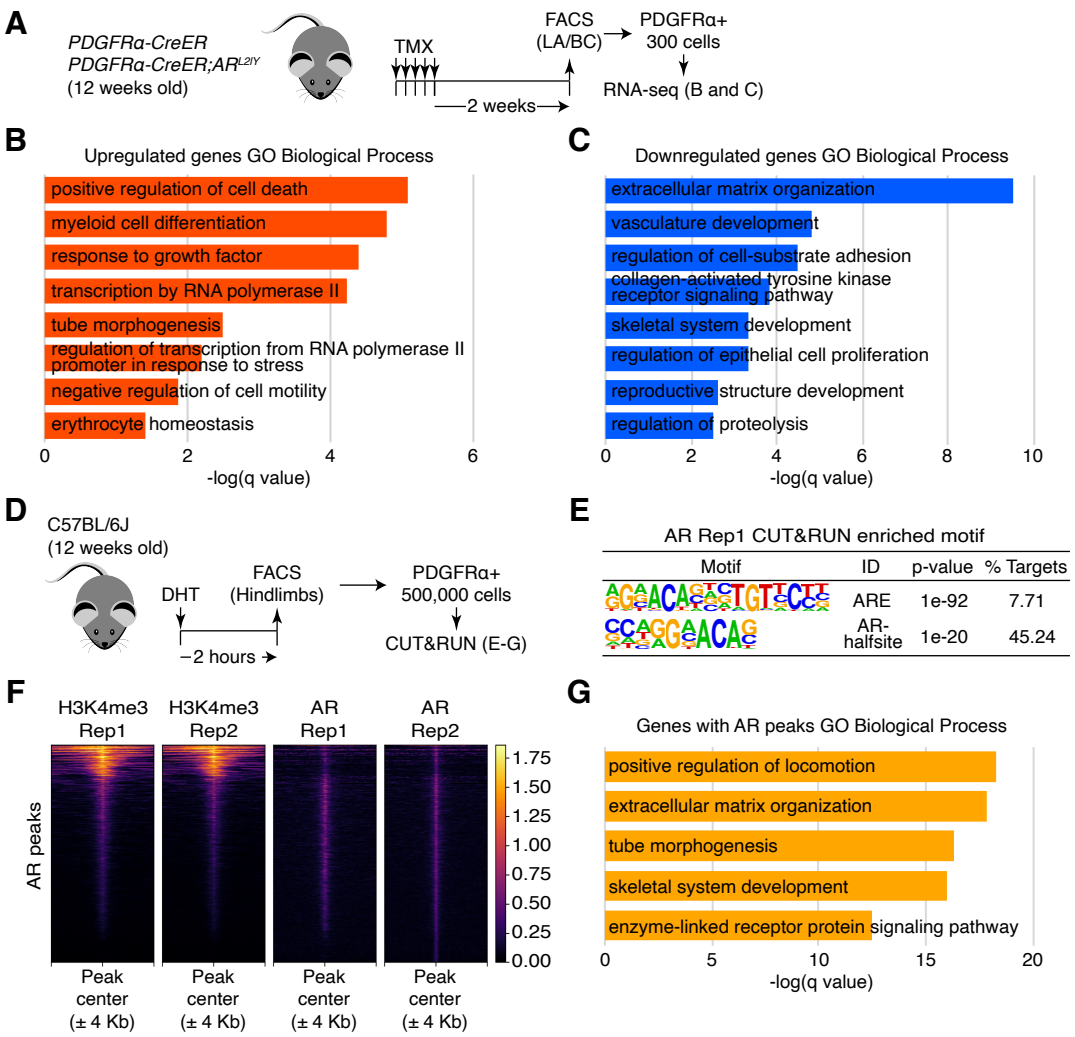

Figure 3. Functional and genomic targets of AR in mesenchymal progenitors of skeletal muscles. (A) Experimental design for tamoxifen (TMX) treatment followed by fluorescence-activated cell sorting (FACS) from levator ani and bulbocavernosus (LA/BC) muscles for RNA-seq. (B and C) Top Gene Ontology (GO) Biological Process terms associated with the upregulated (B) and downregulated (C) genes in PDGFRα+ cells from mutant mice. (D) Experimental design for dihydrotestosterone (DHT) treatment followed by FACS and CUT&RUN. (E) Enriched motifs within AR CUT&RUN peaks. (F) Heatmaps of mean H3K4me3 and AR CUT&RUN counts per million (CPM) normalized read coverage around AR

807 CUT&RUN peaks for individual replicates. (G) Top GO Biological Process terms enriched

808 within AR CUT&RUN peak-associated genes.

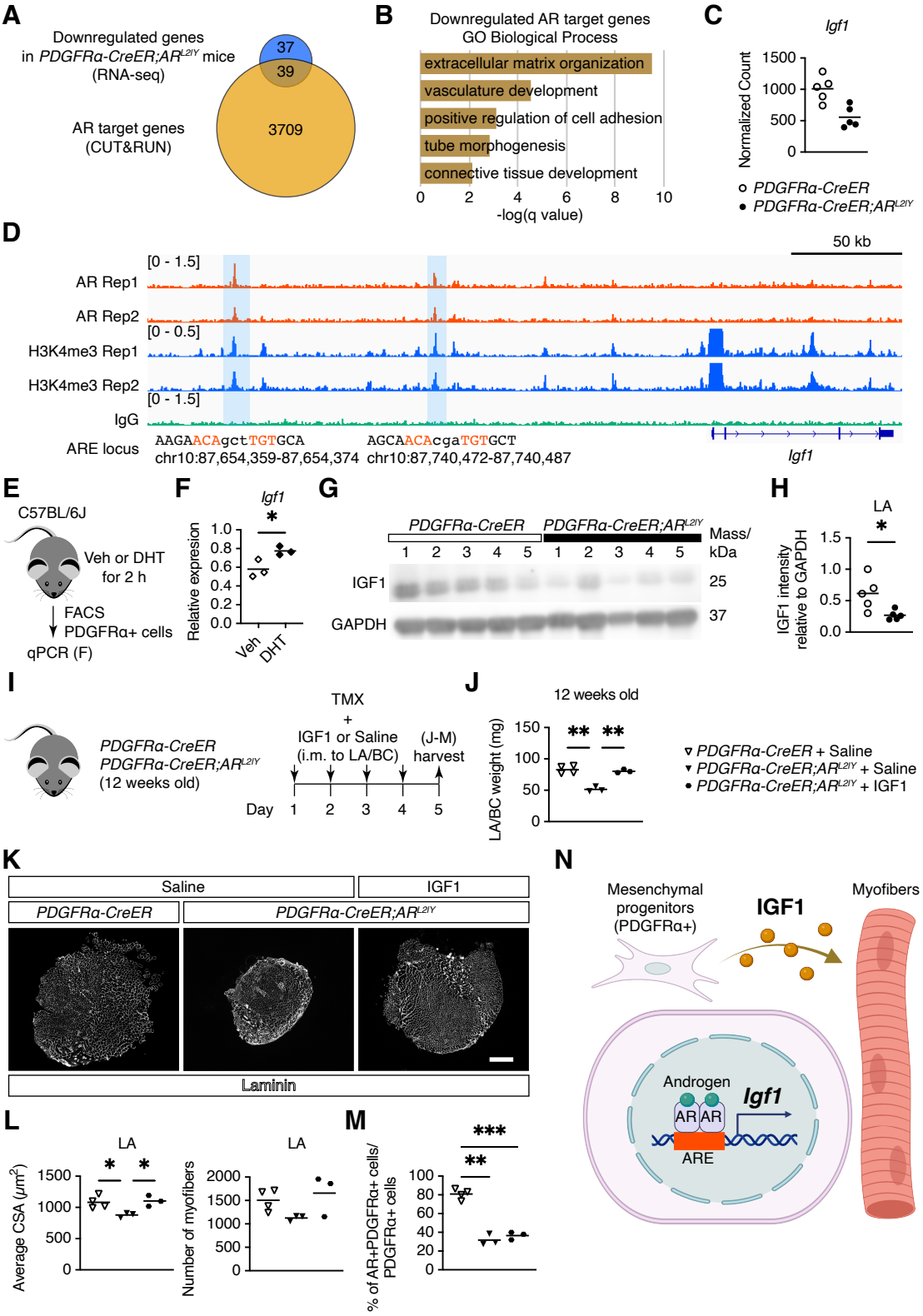
A
Downregulated genes in PDGFRα-CreER;ARL2IY mice (RNA-seq)
AR target genes (CUT&RUN)
37
39
3709
B
Downregulated AR target genes GO Biological Process
extracellular matrix organization
vasculature development
positive regulation of cell adhesion
tube morphogenesis
connective tissue development
-log(q value)
C
Igf1
Normalized Count
PDGFRα-CreER
PDGFRα-CreER;ARL2IY
D
50 kb
AR Rep1
AR Rep2
H3K4me3 Rep1
H3K4me3 Rep2
IgG
ARE locus
AAGAACAGctTGTGCA
chr10:87,654,359-87,654,374
AGCAACAcgaTGTGCT
chr10:87,740,472-87,740,487
Igf1
E
C57BL/6J
Veh or DHT for 2 h
FACS
PDGFRα+ cells
qPCR (F)
F
Igf1
Relative expresion
Veh
DHT
G
PDGFRα-CreER
PDGFRα-CreER;ARL2IY
Mass/ kDa
IGF1
GAPDH
25
37
H
LA
IGF1 intensity relative to GAPDH
I
PDGFRα-CreER
PDGFRα-CreER;ARL2IY
(12 weeks old)
TMX + IGF1 or Saline (i.m. to LA/BC)
(J-M) harvest
Day
J
12 weeks old
LA/BC weight (mg)
PDGFRα-CreER + Saline
PDGFRα-CreER;ARL2IY + Saline
PDGFRα-CreER;ARL2IY + IGF1
K
Saline
IGF1
PDGFRα-CreER
PDGFRα-CreER;ARL2IY
Laminin
N
Mesenchymal progenitors (PDGFRα+)
IGF1
Myofibers
Androgen
AR
AR
Igf1
ARE
L
LA
Average CSA (μm2)
LA
Number of myofibers
M
% of AR+PDGFRα+ cells/ PDGFRα+ cells

809

810 **Figure 4.** Regulation of *Igf1* in mesenchymal progenitors by AR. (A) Overlap of downregulated
811 genes in PDGFRα+ cells from mutant mice and AR CUT&RUN peak-associated genes. (B) Top
812 Gene Ontology (GO) Biological Process terms enriched within overlapped genes. (C)
813 Normalized gene counts for *Igf1* obtained by RNA-seq. (D) AR and H3K4me3 CUT&RUN
814 peaks with androgen response elements (ARE) at *Igf1* locus. The AREs are shown in red. Top
815 left number is the y-axis range in counts per million (CPM). (E) Experimental design for qPCR
816 after treatment with dihydrotestosterone (DHT). (F) qPCR analysis of *Igf1* in PDGFRα+ cells
817 after DHT treatment (n = 3 mice/condition). Unpaired t-test with Welch's correction. (G and H)
818 Western blotting of IGF1 and GAPDH (G) and their quantification (H) in levator ani (LA)
819 muscles from control and mutant mice (n = 5). Unpaired t-test with Welch's correction. (I)
820 Experimental design for intramuscular injection (i.m.) of IGF1 to LA and bulbocavernosus (BC)
821 muscles, followed by tamoxifen (TMX) treatment and sample harvest in 12-week-old control
822 and mutant mice. (J) Mass of LA/BC muscles in saline- or IGF1-injected control and mutant
823 mice (n = 4 control, n = 3 mutant mice with saline or IGF1). Brown-Forsythe and Welch's
824 ANOVA test with Dunnett's T3 multiple comparison test. (K) Immunofluorescence staining of
825 laminin in LA muscles following saline injection in control mice (left), saline injection in mutant
826 mice (middle), and IGF1 injection in mutant mice (right). Scale bar, 500 μm. (L) Average cross-
827 sectional area (CSA) (left) and the number of myofibers (right) in saline- or IGF1-injected
828 control and mutant mice (n = 4 control, n = 3 mutant mice with saline or IGF1). Brown-Forsythe
829 and Welch's ANOVA test with Dunnett's T3 multiple comparison test. (M) Quantification of
830 AR+ cells among PDGFRα+ cells in LA muscles of saline- or IGF1-injected control and mutant
831 mice (n = 4 control, n = 3 mutant mice with saline or IGF1). The three-sample test for equality of

832 proportions: *p < 0.05, **p < 0.01. ***p < 0.001. (N) Regulation of *Igf1* by AR in mesenchymal

833 progenitors of skeletal muscle. Created with BioRender.com.